

Stabilization of Optical Bubbles Near the Axis of a Helical Waveguide

Victor P. Ruban*

Landau Institute for Theoretical Physics RAS, Chernogolovka, Moscow region, 142432 Russia

(Dated: August 13, 2024)

It has been shown numerically that coupled nonlinear Schrödinger equations describing the interaction between the left and right circular polarizations of a paraxial optical wave in a defocusing Kerr medium with an anomalous dispersion in a helical waveguide have stable solutions in the form of elongated stationary rotating bubbles with several optical vortices attached to the ends. A bubble is an arbitrarily long quasi-cylindrical three-dimensional cavity in one of the components filled with the opposite component. The transverse profile of the bubble is determined by the shape of the cross section of the waveguide, the helix pitch, the number of vortices, and the background intensity of the surrounding component rather than by the total amount of the filling component.

DOI: 10.1134/S0021364024602264

Introduction

When studying nonlinear waves, long-lived coherent structures, in particular, solitons and vortices, are of great interest (see, e.g., [1–16], and references therein). New types of such objects are obtained in laboratory and numerical experiments. Multicomponent wave systems are particularly rich in this context and optical systems are the most obvious examples because light can have two independent polarizations. Consequently, it is reasonable to consider an optical wave under “unconventional” conditions in order to possibly detect new effects. The success of this approach is confirmed in this work, where it is shown that the nonlinear interaction between polarizations can form previously unknown wave structures under the action of a special spatial inhomogeneity.

A weakly nonlinear quasi-monochromatic wave propagating paraxially in a wide helical waveguide was chosen for this study because of the formal analogy between nonlinear optics and diluted Bose–Einstein condensates. As known, the paraxial propagation of light with two circular polarizations in a locally isotropic Kerr medium is described by two coupled nonlinear Schrödinger equations [17]. In the case of defocusing nonlinearity and anomalous dispersion, equations in form coincide with Gross–Pitaevskii equations for a binary Bose–Einstein condensate of cold atoms in the phase separation regime [18–24]. A two-component system allows the existence of domain walls separating regions with right and left circular polarization [25–31]. The combination of domain walls and quantized vortices provides interesting three-dimensional structures (see [32–36] and references therein). Stable vortex structures in Bose–Einstein condensates are maintained by the rotation of the trap potential. In optical systems, the (rescaled) coordinate ζ along the light propagation direction rather than the time t serves as the evolution variable, and the helical symmetry of the

waveguide is analog of rotation [37], when the permittivity profile depends on two combinations of the variables:

$$\tilde{x} = x \cos \Omega \zeta + y \sin \Omega \zeta, \quad \tilde{y} = y \cos \Omega \zeta - x \sin \Omega \zeta.$$

In this case, the helix pitch $S = 2\pi/\Omega$ is an analog of the time period of trap rotation. The “retarded” time $\tau = t - \zeta/v_{\text{gr}}$ serves as the third “spatial” coordinate in optical systems. A significant practical difference between Bose–Einstein condensates and light beams is the translational symmetry along this third coordinate in the latter case. Therefore, longitudinally delocalized solutions of equations are not relevant for the physics of cold gases but are directly applicable for optical systems.

Some quasistationary configurations of binary optical beams, where both components of the light wave are nearly “equivalent,” have been numerically obtained in recent work [37]. In this work, stable stationary solutions of a new type — arbitrarily long light “bubbles” (bunches of the conditionally second component inside the conditionally first component), which are confined near the axis of the helical waveguide by several quantized vortices — are obtained. It should be emphasized that the existence of at least two vortices in the first component is necessary. As shown in [35], one vortex cannot confine a large bubble near the axis. The main properties of new three-dimensional structures are theoretically interpreted through the analysis of the energy dependences for strictly two-dimensional solutions with the content n of the second “light fluid” in the presence of Q vortices. The formation of quasi-one-dimensional bubbles is similar to the formation of a condensed phase adjacent to vacuum for an imaginary substance with the energy density $\varepsilon(n)$ if the pressure $p = n^2 d(\varepsilon(n)/n)/dn$ vanishes at a certain finite density n_0 . In other words, the function $\varepsilon(n)/n$ has a nontrivial minimum (at the point where the $\varepsilon(n)$ plot touches a straight line passing through the coordinate origin). The value n_0 strongly depends on the “rotation velocity” Ω , the number of vortices Q , and the corresponding “total density” $n_1 + n$ (see, e.g., plots in Fig. 1). The length of the condensed phase segment can be arbitrary.

*Electronic address: ruban@itp.ac.ru

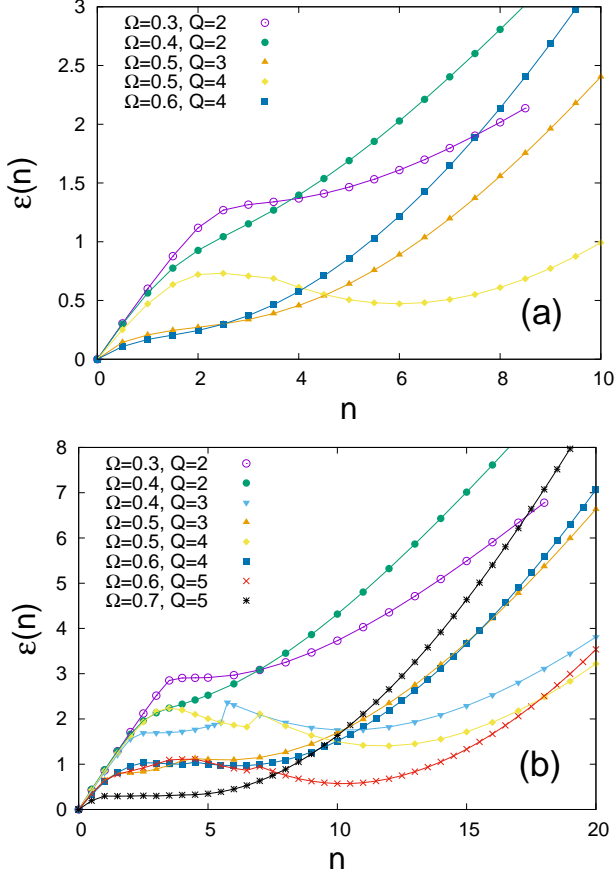


Figure 1: Energy dependences for various rotation velocities and the number of vortices at the total density $n_+ = (n_1 + n) =$ (a) 60.0 and (b) 100.0.

Equations and the numerical method

As in previous works [35, 37], we consider a transparent optical medium with a defocusing Kerr nonlinearity and with the dispersion relation $k(\omega) = \sqrt{\varepsilon(\omega)}\omega/c$ for linear waves and assume the existence of a frequency interval with anomalous dispersion $k''(\omega) < 0$. It is near the low-frequency edge of the transparency window (often the infrared spectral band in real materials; see, e.g., [38, 39]). In this situation, it is possible to apply the known equation for the vector envelope of a weakly nonlinear quasimonochromatic light wave (with the carrier frequency ω_0 ; the complex exponential is chosen in the form $\exp[ik_0\zeta - i\omega_0 t]$) in the paraxial approximation:

$$2k_0[-i\partial_\zeta - ik'_0\partial_t + k''_0\partial_t^2/2]\mathbf{E} - \Delta_\perp\mathbf{E} \approx \frac{k_0^2}{\varepsilon(\omega_0)}[\tilde{\varepsilon}(x, y, \zeta)\mathbf{E} + \alpha|\mathbf{E}|^2\mathbf{E} + \beta(\mathbf{E} \cdot \mathbf{E})\mathbf{E}^*]. \quad (1)$$

Here, $k'_0 = 1/v_{\text{gr}}$ is the inverse group velocity of light in the medium, k''_0 is the negative chromatic dispersion coefficient, $\tilde{\varepsilon}(x, y, \zeta)$ is the small inhomogeneity of the permittivity at the carrier frequency, and $\alpha(\omega_0)$ and $\beta(\omega_0)$

are the negative nonlinear coefficients. The retarded time $\tau = t - \zeta/v_{\text{gr}}$ is introduced as a new variable. The amplitude of the electric field is expressed in terms of the slow amplitudes $A_{1,2}(x, y, \tau, \zeta)$ of the left and right circular polarizations as

$$\mathbf{E} \approx [(\mathbf{e}_x + i\mathbf{e}_y)A_1 + (\mathbf{e}_x - i\mathbf{e}_y)A_2]/\sqrt{2}. \quad (2)$$

Then, the light wave is described by a pair of coupled nonlinear Schrödinger equations [17], similar to a binary Bose–Einstein condensate of cold atoms (with the change in the variables $\zeta \rightarrow t$, $\tau \rightarrow z$). After rescaling, the dimensionless system is obtained in the form

$$i\frac{\partial A_{1,2}}{\partial \zeta} = \left[-\frac{1}{2}\Delta + U(x, y, \zeta) + |A_{1,2}|^2 + g|A_{2,1}|^2\right]A_{1,2}, \quad (3)$$

where $\Delta = \partial_x^2 + \partial_y^2 + \partial_\tau^2$ is the three-dimensional Laplace operator in the “coordinate” space $\mathbf{r} = (x, y, \tau)$, $U \propto -\tilde{\varepsilon}(x, y, \zeta)$ is the external potential, and $g = 1 + 2\beta/\alpha$ is the cross-phase modulation parameter, which is equal to 2 under the assumption of fast nonlinear response. It is substantial that the nonlinear interaction between two components is reduced to a simple incoherent coupling through the coefficient g and keeps the amount of each component $N_{1,2} = \int |A_{1,2}|^2 dx dy d\tau$. Thus, the model describes two quantum compressible liquids with the densities $I_{1,2} = |A_{1,2}|^2$ and velocities $\mathbf{v}_{1,2} = \nabla \text{Arg}(A_{1,2})$.

As in recent work [37], we focus on helical waveguides with a flat bottom and sharp walls. Such waveguides should be easily implemented in experiments, particularly for a liquid Kerr medium. However, for the convenient numerical simulation, the corresponding potential well with the vertical walls is approximated by the expression

$$U = C[1 - \exp(-[(\tilde{x}^2 + \kappa^2\tilde{y}^2)/36]^5)], \quad (4)$$

where $C = 42$ and $\kappa^2 = (1 + 0.3)/(1 - 0.3) = 13/7$ is the transverse anisotropy, which is necessary for the action of the rotation.

It is fundamentally important that Eqs. (3) constitute the Hamiltonian system

$$i\partial A_{1,2}/\partial \zeta = \delta\mathcal{H}/\delta A_{1,2}^*.$$

The corresponding non-autonomous Hamiltonian has the form

$$\begin{aligned} \mathcal{H} &= \frac{1}{2} \int (|\nabla A_1|^2 + |\nabla A_2|^2) dx dy d\tau \\ &+ \int U(x, y, \zeta)(|A_1|^2 + |A_2|^2) dx dy d\tau \\ &+ \frac{1}{2} \int (|A_1|^4 + |A_2|^4 + 2g|A_1|^2|A_2|^2) dx dy d\tau. \end{aligned} \quad (5)$$

This functional is not conserved in the process of evolution. However, since the system in the rotating coordinates is autonomous, the functional

$$\mathcal{H}_\Omega = \mathcal{H} - \Omega \int [A^\dagger(iy\partial_x - ix\partial_y)A] dx dy d\tau, \quad (6)$$

where $A = (A_1, A_2)^T$ is the two-component column, is an integral of motion.

This work is based on the fact that stationary rotating stable solutions of the system of Eqs. (3) are “local minimum points” for the functional \mathcal{H}_Ω (written in the variables \tilde{x} and \tilde{y}) at fixed N_1 and N_2 values.

Equations (3) were numerically simulated using the standard split-step Fourier method of the second order in the evolution variable ζ in the initial (nonrotating) coordinate system. The computational region in the variables x , y , and τ was a $6\pi \times 6\pi \times 12\pi$ rectangular parallelepiped with periodic boundary conditions. However, since the potential well is sufficiently deep, the functions A_1 and A_2 rapidly decrease in the transverse directions to almost zero, so that the effect of transverse boundaries is negligibly small.

The accuracy of calculations was controlled by the conservation of integrals of motion to 4–6 decimal places in the interval $0 < \zeta < 600$ (which corresponds to a propagation length of several tens of meters for a transverse scale of about several tens of wavelengths).

A nearly steady initial state was numerically prepared using a dissipative procedure including two steps in each cycle. The first step corresponded to the purely gradient dissipative dynamics

$$-\partial A_{1,2}/\partial \eta = \delta \mathcal{H}_\Omega / \delta A_{1,2}^*$$

in a narrow range of the auxiliary variable η . In the second step, the functions $A_1(x, y, \tau)$ and $A_2(x, y, \tau)$ are multiplied by suitable factors f_1 and f_2 , respectively, in order to keep the given N_1 and N_2 values, respectively. The total η range was several tens, so that all hard degrees of freedom were effectively suppressed and the system was near the minimum \mathcal{H}_Ω .

Results

Preliminary numerical experiments with the initial conditions in the form of a slightly perturbed filled multiple vortex were first carried out in the free search regime. The subsequent dynamics appeared to significantly depend on the parameters. Only small oscillations near the stable longitudinally homogeneous state were observed in some cases. However, instability was developed in the system at low filling; as a result, the second component was redistributed along the beam axis and characteristic structures in the form of bubbles with several attached “empty” single longitudinal vortices are formed (they are very similar to those shown in Figs. 2 and 3, but less smooth and stationary).

The interpretation of these preliminary experiments required a more detailed study of purely two-dimensional steady states. To find such states with a good accuracy, the typical range of the variable η in the dissipative procedure was several hundreds and sometimes reached thousands. Long-term relaxation occurred in the regime

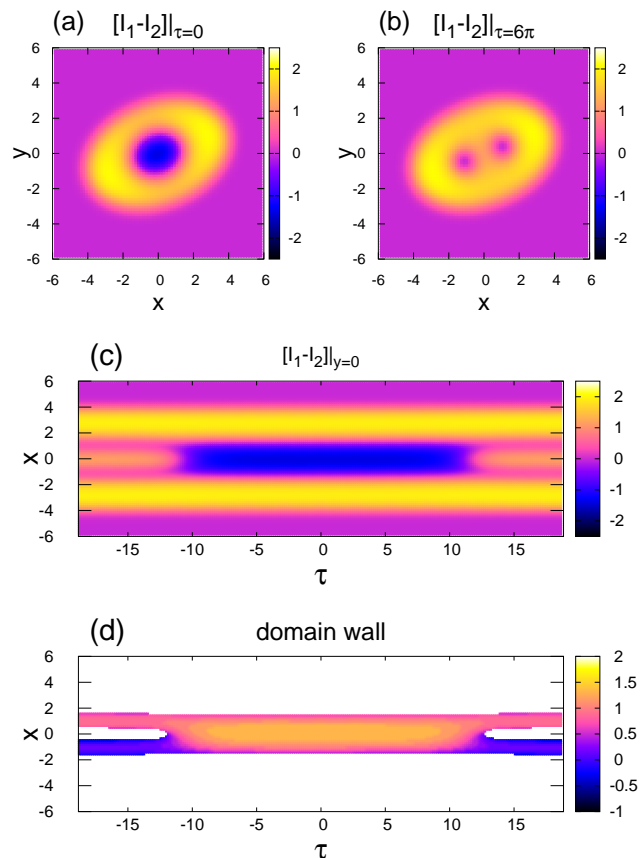


Figure 2: Numerical example of a bubble with two vortices at the “rotation frequency” $\Omega = 0.4$ and the filling factor $\langle n_+ \rangle = 60$ average in the variable τ at the distance $\zeta = 590$: (a) cross section of the light beam through the bubble, (b) cross section through empty vortices, (c) longitudinal section by the $y = 0$ plane, and (d) general side view of the conditional surface of the bubble and vortex filaments attached to it (the color of the points of the numerical lattice near the middle of the domain wall or in the core of the vortex corresponds to the y coordinate perpendicular to the figure plane).

intermediate in the variable $n = \int I_2 dx dy$ between configurations with all almost empty separated vortices on one side and single filled multi-charged vortex at sufficiently large n values on the other side. In this intermediate regime, only some vortices are joined in a filled vortex with a smaller multiplicity and the other vortices “prefer” to be arranged separately (sometimes asymmetrically). The presence of several local minima of the energy functional with their attraction regions can lead to kinks or even jumps on the corresponding dependences of the energy on the variable n . Fortunately, the aims of this work do not require the insight into all these difficulties because the intermediate region is certainly unstable with respect to three-dimensional perturbations. The existence of stable solutions in the regions of small n and sufficiently large n values is practically important.

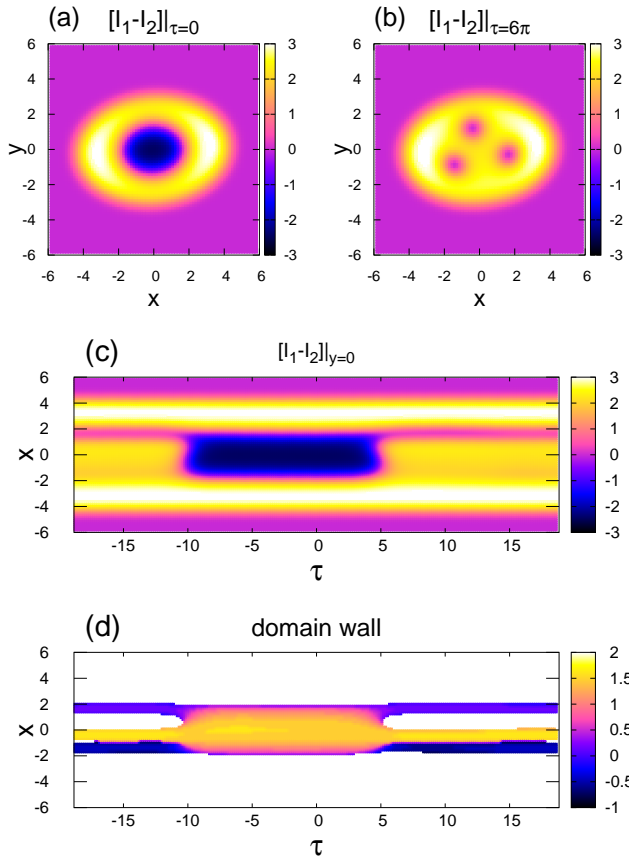


Figure 3: Example of the bubble with three vortices at $\Omega = 0.4$, $\langle n_+ \rangle = 100$, and $\zeta = 550$.

Figure 1 presents the dependences of the energy of two-dimensional solutions on n for different sets of the other parameters including the sum $n_+ = (n_1 + n)$. In each case, the energy at $n = 0$, i.e., in the absence of the second component, was subtracted from the total energy. Strictly speaking, sequences of states with a fixed chemical potential of the first background component are of interest. This condition is practically close to the equality $(n_1 + n) = \text{const}$ (with an accuracy of several percent). This accuracy is quite sufficient for the qualitative analysis.

Most of the plots shown in Fig. 1 have a nontrivial minimum of the ratio $\varepsilon(n)/n$. If $\varepsilon(n)$ is considered as the equation of state of a certain fictitious medium relating its particle number density and the internal energy density, this minimum corresponds to zero pressure. The pressure at slightly higher and lower densities, is positive and negative (i.e., tension), respectively. Consequently, states homogeneous in the variable τ in a certain adjacent n region are stable. However, if “cleavages” are made in a medium with tension, it is collapsed into one-dimensional drops adjacent to “vacuum.” In our three-dimensional system, each such drop is an elongated bubble inside the first component filled with the second component. Two

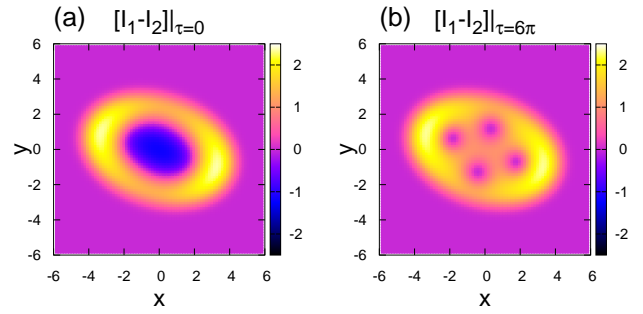


Figure 4: Cross sections of the light beam for the bubble with four vortices at $\Omega = 0.5$, $\langle n_+ \rangle = 60$, and $\zeta = 590$.

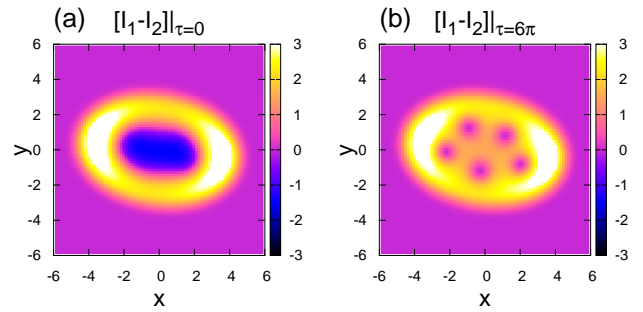


Figure 5: Cross sections of the light beam for the bubble with five vortices at $\Omega = 0.6$, $\langle n_+ \rangle = 100$, and $\zeta = 560$.

steady-state two-dimensional configurations are joined at each of two ends of the bubble; one of them is “vacuum,” i.e., the first component with separated empty vortices and the second configuration is the “medium,” i.e., one multiple vortex with the filled core.

The direct numerical simulation with appropriate initial states confirmed the existence and stability of these structures. The first two examples (for bubbles with two and three vortices) are presented in Fig. 2 and 3, where panels (a–c) demonstrate color maps of the difference between the intensities of the first and second wave components in three different sections of the light beam. Since the phase separation regime occurs (i.e., the product $I_1 I_2$ is negligibly small almost always except for a relatively narrow transient region of the domain wall), regions with a positive difference (bright colors) are filled almost exclusively with the first component, whereas regions with a negative difference (dark colors) are filled primarily with the second component. Therefore, it is not necessary to represent each intensity field individually in figures. The difference $I_1 - I_2$ does not provide complete information only in the domain wall but this information is not too important for the general understanding of the picture. Figures 2d and 3d show the side views of the domain wall, which is the boundary of the bubble, and vortex filaments attached to it. Pictures for bubbles with four

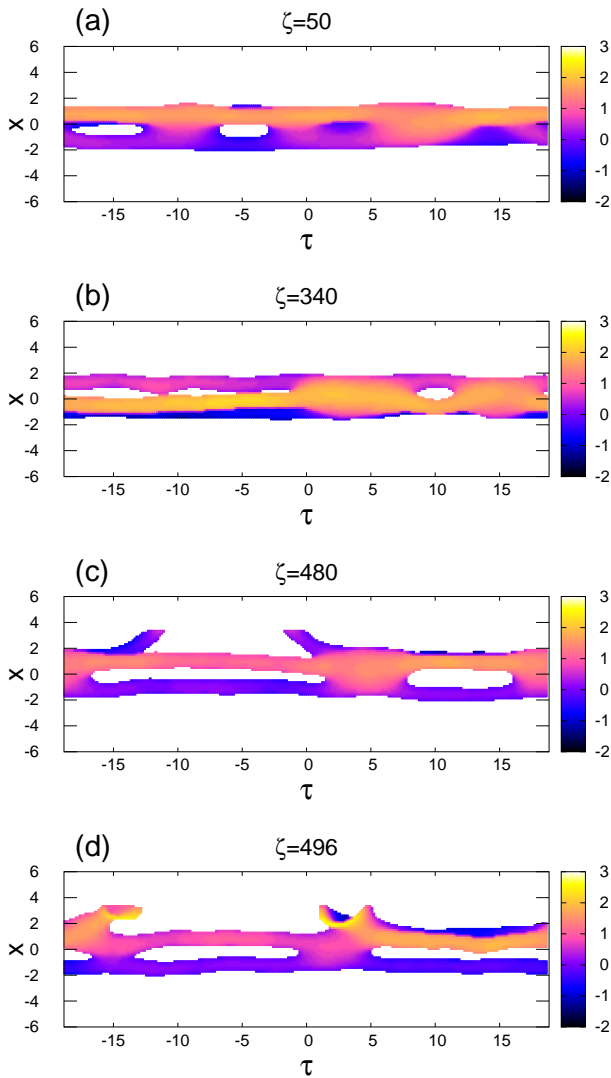


Figure 6: Example of the evolution of the slightly filled triple vortex at the parameters $\Omega = 0.4$ and $\langle n_+ \rangle = 60$ for which the corresponding two-dimensional system does not have a steady-state solution with $n = 0$ in the main stages of (a) the beginning of the formation of bubbles; (b) the appearance of a sufficiently long segment with unfilled vortex filaments; (c) the reconnection of one of the filaments with the waveguide wall (the wall is not shown; for this reason, the filament looks as broken); and (d) the output of the second component from the bubble to the surface of the light beam.

and five vortices are presented in Figs. 4 and 5. Since the structures of all bubbles are qualitatively the same, only cross sections are given in the figures. It is noteworthy that the cross section of bubbles at a large number of vortices is “oblate” and empty vortices are located primarily along an ellipse rather than a circle.

States in all above examples were not strictly steady because small perturbations still remain after the preparational dissipative procedure, but they did not grow at long propagation distances, thus confirming the stable character of the found structures.

It is worth noting that the two-dimensional system of empty vortices is unstable at some parameter values: the width of the waveguide is insufficient to contain vortices, whereas the filled vortex of the corresponding multiplicity is more compact and exists in a wide n range (e.g., at $\Omega = 0.4$, $Q = 3$, $n_+ = 60$, and that is why the corresponding plot is absent in Fig. 1a). In these cases, the “underfilled” three-dimensional vortex first evolves to the formation of a bubble, and then, if deserted segments of vortex filaments are long enough, they gradually approach the waveguide wall and are recoupled to it. The second component leaves through the formed channels to the beam surface. Finally, the entire structure is destroyed. The corresponding example is presented in Fig. 6. Another possible scenario of the development occurs when the bubble itself becomes locally unstable with respect to transverse displacement and is discharged to the waveguide wall (is not shown).

Conclusions

To summarize, the numerical simulation has shown that rotation generated by the helical waveguide strongly changes the dynamics of the optical wave. In particular, it makes the existence of new-type structures theoretically possible. These structures significantly supplement the “collection” of known three-dimensional solitons [2]. Although these results are obtained within the fundamental model given by Eq. (1) they are yet abstract at the current stage. A further work both in theory in order to obtain analytical estimates for $\varepsilon(n)$ etc. and in the selection of materials with the necessary properties for a possible future experiment is necessary. Serious technical difficulties in the way toward the implementation of such an experiment can hardly be foreseen.

Funding

This work was supported by the Ministry of Science and Higher Education of the Russian Federation (state assignment no. FFWR-2024-0013).

Conflict of interests

The author of this work declares that he has no conflicts of interest.

-
- [1] Y. Kivshar and G. P. Agrawal, *Optical Solitons: From Fibers to Photonic Crystals* (Academic, CA, 2003).
- [2] B. A. Malomed, *Multidimensional Solitons*, (AIP, Melville, 2022).
<https://doi.org/10.1063/9780735425118>
- [3] F. Baronio, S. Wabnitz, and Yu. Kodama, Phys. Rev. Lett. **116**, 173901 (2016).
- [4] P. G. Kevrekidis, D. J. Frantzeskakis, and R. Carretero-González, *The Defocusing Nonlinear Schrödinger Equation: From Dark Solitons to Vortices and Vortex Rings* (SIAM, Philadelphia, 2015).
- [5] V. N. Serkin and A. Hasegawa, JETP Lett. **72**, 89 (2000).
- [6] S. K. Turitsyn, N. N. Rozanov, I. A. Yarutkina, A. E. Bednyakova, S. V. Fedorov, O. V. Shtyrina, and M. P. Fedoruk, Phys. Usp. **59**, 642 (2016).
- [7] N. A. Veretenov, N. N. Rozanov, and S. V. Fedorov, Phys. Usp. **65**, 131 (2022).
- [8] S. Raghavan and G. P. Agrawal, Opt. Commun. **180**, 377 (2000).
- [9] B. A. Malomed, D. Mihalache, F. Wise, and L. Torner, J. Opt. B **7**, R53 (2005).
- [10] W. H. Reminger and F. W. Wise, Nat. Commun. **4**, 1719 (2013).
- [11] F. Eilenberger, K. Prater, S. Minardi, R. Geiss, U. Röpke, J. Kobelke, K. Schuster, H. Bartelt, S. Nolte, A. Tünnermann, and T. Pertsch, Phys. Rev. X **3**, 041031 (2013).
- [12] O. V. Shtyrina, M. P. Fedoruk, Y. S. Kivshar, and S. K. Turitsyn, Phys. Rev. A **97**, 013841 (2018).
- [13] S. V. Sazonov, A. A. Kalinovich, M. V. Komissarova, and I. G. Zakharova, Phys. Rev. A **100**, 033835 (2019).
- [14] E. D. Zaloznaya, A. E. Dormidonov, V. O. Kompanets, S. V. Chekalin, and V. P. Kandidov, JETP Lett. **113**, 787 (2021).
- [15] P. Parra-Rivas, Y. Sun, and S. Wabnitz, Opt. Comm. **546**, 129749 (2023).
- [16] V. P. Ruban, JETP Lett. **119**, 585 (2024).
- [17] A. L. Berkhoer and V. E. Zakharov, Sov. Phys. JETP **31**, 486 (1970).
- [18] Tin-Lun Ho and V. B. Shenoy, Phys. Rev. Lett. **77**, 3276 (1996).
- [19] H. Pu and N. P. Bigelow, Phys. Rev. Lett. **80**, 1130 (1998).
- [20] B. P. Anderson, P. C. Haljan, C. E. Wieman, and E. A. Cornell, Phys. Rev. Lett. **85**, 2857 (2000).
- [21] S. Coen and M. Haelterman, Phys. Rev. Lett. **87**, 140401 (2001).
- [22] G. Modugno, M. Modugno, F. Riboli, G. Roati, and M. Inguscio, Phys. Rev. Lett. **89**, 190404 (2002).
- [23] E. Timmermans, Phys. Rev. Lett. **81**, 5718 (1998).
- [24] P. Ao and S. T. Chui, Phys. Rev. A **58**, 4836 (1998).
- [25] M. Haelterman and A. P. Sheppard, Phys. Rev. E **49**, 3389 (1994).
- [26] M. Haelterman and A. P. Sheppard, Phys. Rev. E **49**, 4512 (1994).
- [27] A. P. Sheppard and M. Haelterman, Opt. Lett. **19**, 859 (1994).
- [28] Yu. S. Kivshar and B. Luther-Davies, Phys. Rep. **298**, 81 (1998).
- [29] N. Dror, B. A. Malomed, and J. Zeng, Phys. Rev. E **84**, 046602 (2011).
- [30] A. H. Carlsson, J. N. Malmberg, D. Anderson, M. Lisak, E. A. Ostrovskaya, T. J. Alexander, and Yu. S. Kivshar, Opt. Lett. **25**, 660 (2000).
- [31] A. S. Desyatnikov, L. Torner, and Yu. S. Kivshar, Prog. Opt. **47**, 291 (2005).
- [32] V. P. Ruban, JETP Lett. **113**, 532 (2021).
- [33] V. P. Ruban, J. Exp. Theor. Phys. **133**, 779 (2021).
- [34] V. P. Ruban, JETP Lett. **116**, 329 (2022).
- [35] V. P. Ruban, JETP Lett. **117**, 292 (2023).
- [36] V. P. Ruban, JETP Lett. **117**, 583 (2023).
- [37] V. P. Ruban, J. Exp. Theor. Phys. **137**, 746 (2023).
- [38] X. Liu, B. Zhou, H. Guo, and M. Bache, Opt. Lett. **40**, 3798 (2015).
- [39] X. Liu and M. Bache, Opt. Lett. **40**, 4257 (2015).